Direct evidence for a steep geotherm under conditions of rapid denudation, Western Himalaya, Pakistan

David M. Winslow, Peter K. Zeitler
Department of Earth and Environmental Sciences, 31 Williams Drive, Lehigh University, Bethlehem, Pennsylvania 18015
C. Page Chamberlain
Department of Earth Sciences, Dartmouth College, Hanover, New Hampshire 03755
Lincoln S. Hollister
Department of Geological and Geophysical Sciences, Princeton University, Princeton, New Jersey 08544

ABSTRACT

Recent fluid-inclusion and $^{40}Ar/^{39}Ar$ cooling-age data show that currently exposed basement rocks in the Raikhot glacier valley of the Nanga Parbat–Haramosh massif, Pakistan Himalaya, were at temperatures of 350 ± 50 °C at depths of 6 ± 2 km (hydrostatic pressure correction). These data imply the presence of a steep thermal gradient in the upper crust at 1 Ma (29–100 °C/km) and denudation rates over the past 1.0 m.y. of 3–6 mm/yr, providing independent corroboration of previous estimates of rapid denudation at Nanga Parbat (4.5 mm/yr over 3.3 m.y.). Our data provide direct documentation of near-surface compaction of isotherms under conditions of rapid denudation, a result that has long been supported by thermal modeling.

INTRODUCTION

Previous geologic studies (Hollister, 1979; Hollister 1982; Selverstone, 1988; Craw, 1988), which have incorporated results from fluid-inclusion studies, have shown that mountain belts undergoing rapid denudation at rates of >1 mm/yr had pronounced thermal perturbations characterized by elevated isotherms at shallow crustal levels. This fact has been supported by thermal models (Oxburgh and Turcotte, 1974; Alberede, 1976; England and Thompson, 1984; Koons 1987). This paper presents quantitative documentation of the near-surface packing of isotherms in a young terrane undergoing rapid denudation.

We report homogenization- and melting-temperature data on secondary trails of fluid inclusions that crosscut grain boundaries of dynamically recrystallized quartz. Entrapment of the inclusions is thus determined to have occurred after grain-boundary migration in quartz had ceased. These data provide minimum and maximum entrapment conditions that, when combined with $^{40}Ar/^{39}Ar$ cooling ages on biotite (Winslow et al., 1993, 1994), provide quantitative controls on the Quaternary denudation and thermal evolution of the Nanga Parbat–Haramosh massif.

GEOLOGIC SETTING

The Nanga Parbat–Haramosh massif (Fig. 1) is a north-trending promontory of Indian basement. The massif is bordered on the west by the north-trending Raikhot fault that juxtaposes Indian basement over Cretaceous rocks of the Kohistan sequence (Treloar et al., 1991; Madin et al., 1989; Butler et al., 1989). Butler et al. (1989) have presented kinematic evidence for dextral reverse motion along the Raikhot fault. To the north (not shown in Fig. 1), features along the fault show an oblique dextral sense of movement, with east side up on vertical surfaces (Butler et al., 1989).

Madin et al. (1989) have shown that the dominant ductile structures within the massif are three generations of folding, characterized by transposition of a previous fabric to an S1 fabric that has left only highly attenuated isoclinal folds of an earlier F1 event (Madin et al., 1989). F2 structures are present along the Indus gorge as an antiform-synform pair with east-trending axes.

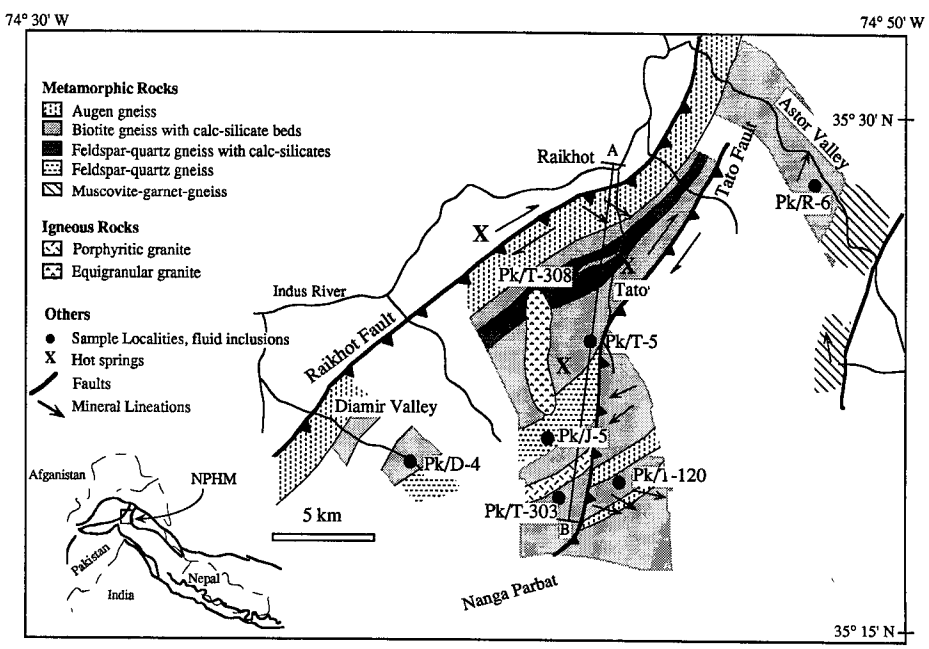

Figure 1. Simplified geologic map of study area showing geologic relations as well as fluid-inclusion sample locations and location of biotite cooling-age traverse (A–B). NPHM—Nanga Parbat–Haramosh massif.

F3 folds are northeast-trending upright, tight, asymmetric antiforms with steeply dipping western limbs and gently dipping eastern limbs. Uplift along the Raikhot fault system correlates with the F3 event (Madin et al., 1989).

Mineral lineations within the massif vary in orientation. Treloar et al. (1991) reported a detailed structural study along the Indus gorge, to the north of our study area. They showed that mineral lineations are predominantly north-south, and they attributed these to an early Himalayan or Precambrian metamorphism. Along the Raikhot fault, the lineations are oriented about an east-west axis as a result of recent denudation of the massif. We find that within the migmatized region of the massif, in the Raikhot valley, the mineral lineations are also oriented east (Fig. 1). We infer these lineations to represent an east-west transport direction associated with denudation of the massif.

Timing of metamorphism and denudation of the massif has been determined by isotopic dating. Zeitler et al. (1993) reported U/Pb ages on zircons and monazites from the migmatized region in the Raikhot valley to be as young as 3.3 Ma. Farther to the north, the U/Pb monazite ages increase to 10–12 Ma (Smith et al., 1993). Maximum Sm/Nd final equilibration ages on garnet, from the Astor valley, are <25 Ma and possibly as young as 10–12 Ma (Nigel Harris, 1994, personal commun.). These ages are in good agreement with the U/Pb ages on monazite.

Winslow et al. (1993, 1994) presented $^{40}Ar/^{39}Ar$ total-fusion ages on biotite separates, along a north-south traverse of the Raikhot glacial valley. These ages decrease toward the summit region of the massif. Ages as young as 0.85 ± 0.02 Ma have been recorded within the summit region (Fig. 2). One kilometre south of the Raikhot fault, biotite grains record $^{40}Ar/^{39}Ar$ cooling ages of 1.8 ± 0.1 Ma. The ages decrease to 1.06 ± 0.02 Ma within 0.5 km and then steadily increase to over 4.0 Ma over a distance of 3 km. At the Tato fault, ages drop off sharply to 1.60 ± 0.01. Step-heated analysis of older samples shows, however, that the older total-fusion ages south of the Tato fault are related to excess-Ar incorporation, and the resulting ages more closely match the overall pattern but represent maximum cooling ages. The two oldest samples from between the Tato and Raikhot faults decrease by only 0.5 and 0.3 Ma after step heating, indicating that the age pattern in this region is real. George et al. (unpublished manuscript) have suggested that leucogranites intruded the massif while the country rocks were at or above the closure temperature of biotite.

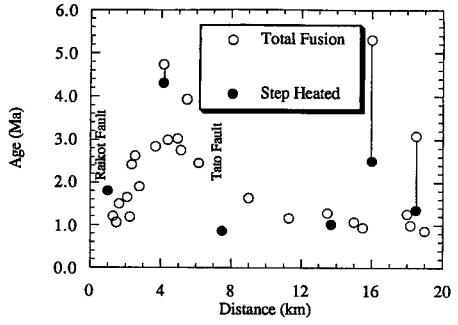

Figure 2. $^{40}Ar/^{39}Ar$ cooling ages on biotites along line A–B in Figure 1. Ar data are projected onto the straight line. Open circles represent total-fusion cooling ages and show age minimum of 0.8 Ma and maximum of 4.8 Ma; errors are within limits of symbols used. Cooling ages steadily increase away from Raikhot fault and then drop sharply at Tato fault. Solid circles represent inverse-correlation ages from step-heated samples. Lines between solid and open circles connect samples for which both types of experiments were performed. Step heating reveals that age difference between Raikhot and Tato faults is real. The old ages south of Tato fault are due to incorporation of excess Ar.

PETROGRAPHY

Samples

Samples were collected from in situ migmatites, pegmatitic dikes, quartz veins, and orthogneisses across the Nanga Parbat massif. This area has been affected by cordierite + K-feldspar + sillimanite granulite-grade metamorphism in the summit region of Nanga Parbat. On the flanks of the massif, metamorphism occurred in the kyanite + muscovite stability field.

Pegmatitic dikes contain scattered grains of euhedral (rectangular) plagioclase as well as feldspars that have undergone recrystallization. Quartz-grain boundaries are lobate and sutured. Locally, quartz grains exhibit diffuse undulatory extinction. Quartz-grain sizes vary from 50 to 500 μm in diameter. Generally, small quartz grains appear to be strain free. The microstructural development is similar to that described by Hirth and Tullis (1992) as indicating recrystallization at low temperatures.

Quartz veins also exhibit similar microstructures. Some of the large quartz crystals exhibit a patchy undulatory extinction. Locally, small (~50 μm) recrystallized grains rim the larger grains. Grain-boundary migration is apparently the dominant recrystallization process as indicated by lobate grain boundaries. Microfracturing is common throughout the veins. In some cases the microfractures cut the grain boundaries; in other cases the microfractures terminate at the lobate grain boundary.

Fluid Inclusions

The fluid inclusions (Table 1) contain either two or three phases at room temperature, are generally <25 μm in diameter, and show no signs of having been formed from closing of larger inclusions (necking down). The presence of fluid inclusions in microfractures (30–300 μm thick and traversing several grains) limits the entrapment of the secondary planes to temperatures at or below the brittle-ductile transition, following formation of the quartz grain boundaries (Kerrich, 1976; Craw, 1988; Hollister, 1990; Craw and Norris, 1993; Johnson and Hollister, 1994). Locally, grain boundaries, which are crosscut by secondary trails, are decorated by low-salinity aqueous fluid inclusions.

Sample Pk/J-5 contains small (<30 μm in diameter) fluid inclusions found in nonplanar as well as planar arrays. The fluid inclusions are oval to faceted and are composed of vapor-rich and liquid-rich fluid compositions. The room-temperature phase ratios of both the liquid- and vapor-rich inclusions are constant, arguing against necking down as a mechanism for the formation of two distinct fluid-inclusion compositions.

RESULTS

Fluid-inclusion compositions and densities were determined through the use of standard heating and freezing measurements on a Fluid Inc. gas-flow heating and freezing stage. Measured temperatures have accuracies of ±0.2 °C at temperatures of ≤50 °C and ±2.5 °C at temperatures of about 375 °C. Salinities (NaCl equivalent) of aqueous inclusions were determined from freezing-point depressions of H_2O, and compositions were calculated from the eutectic temperature (first melting of ice) of the solution. Densities of H_2O-NaCl and CO_2-H_2O-NaCl inclusions were calculated using the equation of state of Bowers and Helgeson (1983) and the program MacFlincore. Table 1 shows the sample identification number, lithology, homogenization and melting data, and inferred entrapment conditions associated with the locality.

Commonly, CO_2-H_2O fluid inclusions have X_{CO_2} = 0.15–0.36 and range in salinity from 0 to only 0.1 wt% NaCl equivalent. The inclusions (Fig. 3) showed total homogenization to both liquid and vapor at temperatures between 301 and 360 °C, corresponding to densities between 0.366 and 0.854 $g \cdot cm^{-3}$. All inclusions contain three phases at room temperature except those from a quartz-vein sample in Diamir Valley, which contain two phases at room temperature.

H_2O-NaCl fluid inclusions contain two phases at room temperature and have melting temperatures between −1.3 °C and

TABLE 1. FLUID INCLUSION DATA

Sample	n	T_{mbr}	T_{hbr}	T_{mCO2}	T_{hCO2}	T_{mcl}	T_{hf}	Size	Mode	Inferred Temperature (°C)	Inferred Pressure (bar)
Pk/T120	9	-1.6	277.3 (l)					12	Trail	277-400	70-1000
	10			57.6	28.3 (v)	8.2		9	G.B		
	10	-0.1	276.5 (l)						G.B	>277	>70
Pk/T308	13			-58.5	21.5 (l)	10.0	331.1 (l)	18	Group		
	9	-2.8	313.0 (l)					6	Trail	313-400	
Pk/J-5	17	-1.7	270.2 (l)					6	Trail	270-300	
	7	-1.3	352.1 (l)					15	Group	~350	~150
	9	-0.1	354.1 (v)					18	Group	~350	~150
Pk/T303	14			-57.1	29.3 (v)	10.0	306.0 (v)	20	Trail	300-400	375-700
Pk/R-6				-57.0	27.3 (l)	9.6	309.4 (v)	25	Trail	285-400	800-1400
	12	-3.2	257.0 (l)						Trail	256-400	
Pk/D-4				-59.8	02.6 (v)	10.2	375.3 (v)	30	Trail	~400	~300
	15	-1.5	265.0 (l)						Trail	265-400	65-850

Note: N = number of inclusions analyzed; T_{mbr} = melting temperature of the brine; T_{hbr} = temperature at which only a single phase was present in the brine; T_{mCO_2} = temperature at which solid CO_2 melted; T_{hCO_2} = temperature at which CO_2 was all one phase; T_{mcl} = melting temparature of the clathrate; T_{hf} = temperatre at which homogenization of all phases occurred; G.B. = grain boundary; v = vapor; l = liquid.

−2.6 °C, corresponding to a salinity of ~3–5 wt% NaCl equivalent. First-melting temperatures of these inclusions could not be determined owing to their small size; thus, we cannot preclude the presence of other dissolved cations within the fluid inclusions that would affect the calculated salinity and densities of the trapped fluid. However, given the low salinities of the fluid inclusions, even a pure $CaCl_2$ salt component would shift the isochores by only a few 10s of bars. These inclusions homogenize to the liquid between 250 and 330 °C.

The inclusions from sample Pk/J-5 from Tato Valley homogenize to liquid or vapor in the narrow range between 348 °C and 363 °C. Inclusions homogenizing to vapor are pure water with melting temperatures of 0 ± 0.1 °C, whereas inclusions homogenizing to liquid have melting temperatures between −2.0 °C and −1.6 °C. The presence of inclusions that homogenize to either liquid or vapor is indicative of entrapment of a boiling fluid.

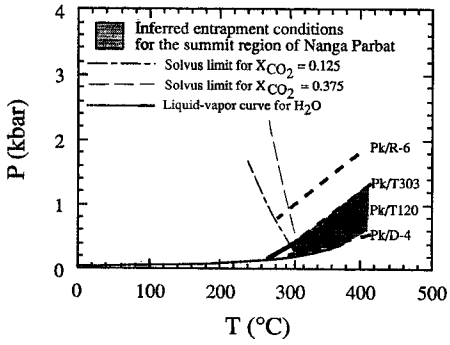

Figure 3. Plot of isochores for CO_2-H_2O-and H_2O-NaCl-rich fluid inclusions analyzed from Tato section. Shaded region represents range in conditions of entrapment. Short dashed lines are isochores for CO_2-H_2O. These isochores terminate on the low-temperature end at the position of the CO_2-H_2O immiscibility curve for their respective compositions and densities. Solid lines represent isochores for H_2O-NaCl, and long-dashed lines represent the solvus for CO_2-H_2O.

TEMPERATURE AND DEPTH OF ENTRAPMENT

The fluid inclusions that best indicate entrapment conditions occur along healed microfractures that postdate grain-boundary migration in quartz. The presence of microfractures that both crosscut and do not crosscut grain boundaries of dynamically recrystallized quartz provides us with a maximum temperature of entrapment, the intersection of the secondary fluid-inclusion isochores with the brittle-ductile transition. We have taken the brittle-ductile transition in quartz to be 300–400 °C at geologic strain rates (Sibson et al., 1979; Knipe, 1989; Johnson and Hollister, 1994). According to Butler et al. (1989), deformation along the Raikhot fault system was continuous from amphibolite conditions through the brittle-ductile transition. Treloar et al. (1991) suggested that the main fabric within the interior of the massif may be Precambrian or Himalayan (55–20 Ma) and may have been passively uplifted. Alternatively, Smith et al. (1993) and Zeitler et al. (1993) have shown that monazites, included in biotites, with no obvious features associated with hydrothermal alteration, record Neogene U/Pb ages as young as 3.3 Ma, indicating that growth of the metamorphic fabric occurred at this time. Furthermore, our ongoing structural studies indicate that within the migmatized region of the massif, the rocks underwent recrystallization associated with development of the east-trending mineral lineations. This implies that plastic deformation was occurring over the past 3.3 m.y. and that the fluid-inclusion trails found within the pegmatite and migmatite leucosomes were trapped after or during this recrystallization event. The minimum entrapment conditions for the H_2O-CO_2 fluid-inclusion trails can be determined by the position of the H_2O-CO_2 solvus (Sterner and Bodnar, 1991).

Although the determination of whether lithostatic or hydrostatic pressures prevailed during entrapment of the fluid inclusions is not critical to the interpretation of our data, we have attempted to determine which pressures dominated at the time of entrapment. The fluid-inclusion trails were trapped at or below the brittle-ductile transition, which may suggest either hydrostatic or lithostatic pressures. However, lithostatic corrections imply exceptionally high near-surface thermal gradients (as high as 240 °C/km). The use of hydrostatic corrections yields more reasonable geothermal gradients and denudation rates, which are in agreement with rates reported elsewhere (Zeitler et al., 1993). In any event, the use of either pressure correction leads to the conclusion that the geotherm was relatively steep at the time of entrapment.

To quantify the geothermal gradient during denudation, we have chosen to take the average entrapment conditions as deduced through fluid-inclusion techniques and apply a hydrothermal pressure correction to arrive at depths. We have utilized fluid-inclusion data from the Tato region to determine the geothermal gradient as this is the region showing the most pronounced thermal effects (Zeitler et al., 1993; Winslow et al., 1994). Our minimum conditions were defined by the location of the H_2O-CO_2 solvus, 300–380 bar at ~300 °C. The maximum conditions were determined as 700–1400 bar at 400 °C. This leads to a range of geothermal gradients of 29–57 °C/km at the up-

per temperature limit and 80–100 °C/km at the lower temperature limit. The upper-temperature-limit depths may be too high, given that this is a high estimate for the brittle-ductile transition. Therefore, we have decided to report the average depth (6 km) at 350 °C to determine the average geothermal gradient during denudation of the Tato region, 58 °C/km.

The relation between biotite cooling ages and fluid-inclusion entrapment conditions is not entirely clear. Previous workers have gathered thermochronologic data suggesting at least 15 km of denudation over the past 10 m.y. (Zeitler, 1985; Treloar et al., 1991). These authors arrived at these denudation rates by assuming a geothermal gradient lower than the one we have documented. This would result in an underestimation of the amount of denudation over the past 10 Ma. Therefore, the fluid inclusions must have formed earlier than 10 Ma because the amount of denudation since this time would undoubtedly have removed the former brittle section of the crust. The closure of biotite to Ar diffusion at high cooling rates is within the temperature range commonly reported for the brittle-ductile transition (Sibson et al., 1979). When the fluid-inclusion data are combined with $^{40}Ar/^{39}Ar$ biotite cooling age data, denudation rates of 6 ± 2 mm/yr (hydrostatic pressure corrections) are concluded to have occurred within the Nanga Parbat region of the massif over the past 1 m.y.

CONCLUSIONS

The Nanga Parbat–Haramosh massif is currently undergoing denudation, resulting in a higher than normal geotherm (~58 °C/km) due to rapid advection of hot rocks from depth. We have documented that this steepened geotherm existed as recently as 1 Ma. Comparable results have recently been obtained from other areas that have undergone rapid denudation (Hollister, 1979; Craw, 1988; Johnson and Hollister, 1994). The Nanga Parbat massif has experienced an average denudation rate of 6 ± 2 mm/yr (hydrostatic) from ~1.0 Ma to the present. These high denudation rates resulted in an elevated thermal gradient as heat was advected close to the surface faster than it could be dissipated by conduction alone, producing the high geothermal gradient found within the Nanga Parbat–Haramosh massif. The pronounced denudation rates documented in the Nanga Parbat–Haramosh massif are either due to erosion or extension, or a combination of the two. Denudation not aided by extension would imply exceptionally high erosion rates. Although significant erosion in the massif area is obvious, the role of extension in the denudation of the massif must still be evaluated.

ACKNOWLEDGMENTS

Supported by Geological Society of America grant 5085-92 (Winslow), National Science Foundation grants EAR-8957703 and EAR-881629 (Chamberlain), EAR-881687 and EAR-9105878 (Zeitler), and the Kiewit Foundation. We thank David Craw for his comments and suggestions on an earlier manuscript; Mike Krol for his assistance in the field and for helpful discussions; and Marry Hubbard, Peter Treloar, Jane Selverstone, and an anonymous reviewer for helpful reviews of this manuscript.

REFERENCES CITED

Alberede, F., 1976, Thermal models of post-tectonic decompression as exemplified by the Haut-Allier granulites (Massif Central, France): Société Géologique de France, Bulletin, v. 18, p. 1023–1032.

Bowers, T. S., and Helgeson, H. C., 1983, Calculation of the thermodynamic and geochemical consequences of nonideal mixing in the system H_2O-CO_2-NaCl on phase relations in geological systems: Equation of state for H_2O-CO_2-NaCl fluids at high pressures and temperatures: Geochimica et Cosmochimica Acta, v. 47, p. 1247–1275.

Butler, R. W. H., Prior, D. J., and Knipe, R. J., 1989, Neotectonics in the Nanga Parbat syntaxis, Pakistan, and crustal staking in the northwest Himalayas: Earth and Planetary Science Letters, v. 94, p. 329–343.

Craw, D., 1988, Shallow-level metamorphic fluids in a high uplift rate mountain belt, Alpine Schist, New Zealand: Journal of Metamorphic Geology, v. 6, p. 1–16.

Craw, D., and Norris, R. J., 1993, Grain boundary migration of water and carbon dioxide during uplift of garnet-zone Alpine Schist, New Zealand: Journal of Metamorphic Geology, v. 11, p. 371–378.

England, P. C., and Thompson, A. B., 1984, Pressure-temperature-time paths of regional metamorphism. I: Heat transfer during the evolution of regions of thickened continental crust: Journal of Petrology, v. 25, p. 894–928.

Hirth, G., and Tullis, J., 1992, Dislocation creep regimes in quartz aggregates: Journal of Structural Geology, v. 14, p. 145–159.

Hollister, L. S., 1979, Metamorphism and crustal displacements: New insights: Episodes, v. 1979, p. 3–8.

Hollister, L. S., 1982, Metamorphic evidence for rapid (2 mm/yr) uplift of a portion of the central gneiss complex, Coast Mountains, B.C.: Canadian Mineralogist, v. 20, p. 319–332.

Hollister, L. S., 1990, Enrichment of CO_2 in fluid inclusions in quartz by removal of H_2O during crystal plastic deformation: Journal of Structural Geology, v. 12, p. 895–901.

Johnson, E. L., and Hollister, L. S., 1994, Syndeformational fluid trapping in quartz: Determining the pressure and temperature conditions of deformation from fluid inclusions and the formation of pure CO_2 fluid inclusions during grain boundary migration: Journal of Metamorphic Geology (in press).

Kerrich, R., 1976, Some effects of tectonic recrystallization on fluid inclusions in vein quartz: Contributions to Mineralogy and Petrology, v. 59, p. 195–202.

Knipe, R. J., 1989, Deformation mechanisms—Recognition from natural tectonites: Journal of Structural Geology, v. 11, p. 127–146.

Koons, P. O., 1987, Some thermal and mechanical consequences of rapid uplift: An example from the Southern Alps, New Zealand: Earth and Planetary Science Letters, v. 86, p. 307–319.

Madin, I. P., Lawrence, R. D., and Ur-Rehman, S., 1989, The northwestern Nanga Parbat–Haramosh Massif: Evidence for crustal uplift at the northwest corner of the Indian craton, *in* Malinconico, L. L., and Lillie, R. J., eds., Tectonics of the western Himalayas: Geological Society of America Special Paper 232, p. 169–182.

Oxburgh, E. R., and Turcotte, D. L., 1974, Thermal gradients and regional metamorphism in overthrust terranes with special references to the eastern Alps: Schweitzerische Mineralogische und Petrographische Mitteilungen, v. 54, p. 641–662.

Selverstone, J., 1988, Evidence for east-west crustal extension in the eastern Alps: Implications for the unroofing history of the Tauren Window: Tectonics, v. 7, p. 87–105.

Sibson, R. H., White, S., and Atkinson, B. K., 1979, Fault rock distribution and structure within the Alpine fault zone: A preliminary account, *in* Walcot, R. I., and Cresswel, M. M., ed., The origin of the Southern Alps: Royal Society of New Zealand Bulletin, v. 18, p. 55–66.

Smith, H., Chamberlain, C. P., and Zeitler, P. K., 1993, Documentation of Neogene regional metamorphism in the Himalayas of Pakistan using U-Pb in monazite: Earth and Planetary Science Letters, v. 113, p. 93–106.

Sterner, M. S., and Bodnar, R. J., 1991, Synthetic fluid inclusions. X: Experimental determination of the *P-V-T-X* properties in the CO_2-H_2O system to 6 kbar and 700 °C: American Journal of Science, v. 291, p. 1–54.

Treloar, P. J., Potts, G. J., Wheeler, J., and Rex, D. C., 1991, Structural evolution and asymmetric uplift of the Nanga Parbat syntaxis, Pakistan Himalaya: Geologische Rundschau, v. 80, p. 411–428.

Winslow, D. M., Zeitler, P. K., and Chamberlain, C. P., 1993, Combined $^{40}Ar/^{39}Ar$ biotite cooling ages and fluid inclusion data from Nanga Parbat (Pakistan Himalaya); an indication of the depth to paleoisotherms with time: EOS (Transactions, American Geophysical Union), v. 74, p. 301.

Winslow, D. M., Zeitler, P. K., and Chamberlain, C. P., 1994, Petrology, thermochronology and fluid inclusions: Implications for the denudation and metamorphic history of the Nanga Parbat region, Pakistan: EOS (Transactions, American Geophysical Union), v. 75, p. 186.

Zeitler, P. K., 1985, Cooling history of the northwestern Himalaya, Pakistan: Tectonics, v. 4, p. 127–151.

Zeitler, P. K., Chamberlain, C. P., and Smith, H., 1993, Synchronous anatexis, metamorphism, and rapid denudation at Nanga Parbat (Pakistan Himalaya): Geology, v. 21, p. 247–250.

Manuscript received June 6, 1994
Revised manuscript received August 29, 1994
Manuscript accepted September 7, 1994